PII: S0955-2219(98)00103-4

0955-2219/98/$—see front matter

X-ray Absorption Spectroscopy: A Tool to Study the Local Atomic and Electronic Structure of Ceramics

Martine Gautier-Soyer

CEA Saclay, DSM/DRECAM/SRSIM, 91191 Gif sur Yvette Cedex, France

(Received 12 November 1997; revised version received 16 March 1996; accepted 20 March 1998)

Abstract

X-ray absorption spectroscopy (XAS) is a powerful tool for investigating the local atomic and electronic structure around selected types of atoms in materials, independently of the presence of long or medium range order. We show on several examples, how XAS can bring useful information in the case of ceramic materials, when combined to theoretical modelling of the absorption spectra. Local structure around Ce doping atoms in Y_2O_3, structural modifications of PbO during the α–β phase transformation are presented first. We illustrate in the case of iron oxides, the possibilities offered by XAS at different edges (Fe and O K, Fe L_{23}) in determining both the valence and site symmetry of the iron atoms. We conclude with the perspectives provided by the third generation synchrotron sources in the field of microanalysis by XAS.

1 Introduction

X-ray absorption spectroscopy (XAS) has become an essential tool to extract structural and electronic information on a wide range of materials, thanks to the development of experimental synchrotron radiation sources. This method presents important assets:

- It allows characterisation of the local order in every material, whatever its crystalline state. No long range order is needed.
- Each atom of the material can be probed separately (chemical selectivity).
- With appropriate experimental devices, the study of dynamic processes is possible, for example phase transformations produced by varying pressure or temperature.

Moreover, the intrinsic polarisation features of the X-ray beam produced by synchrotron radiation sources can be exploited to do dichroism experiments, which are widely developing in the field of magnetic materials.

The present paper is intended to illustrate the possibilities offered by XAS in the field of ceramics. In the first part, we briefly recall the physical basis of the method, by making the usual distinction between EXAFS (Extended X-ray Absorption Fine Structure) and XANES (X-ray Absorption Near Edge Structure), and the principles of XAS data collection. The second part deals with EXAFS. Two examples are taken: the determination of local order in Ce doped Y_2O_3 ceramics, and a dynamic study of the $\alpha \rightarrow \beta$ phase transition mechanism of PbO. The third part, devoted to XANES, shows in the case of iron oxides, what kind of information (valence and site symmetry) can be gained from the near edge structures. Knowing reference spectra at different edges, it is possible to use them as a fingerprint of the valence and site symmetry, so as to characterise unknown samples or to follow phase transformations. Last part deals with the possible use of XAS as a microprobe of the local order around selected atoms and with the perspectives opened in the field of micro-XANES by the high brilliance third generation synchrotron sources.

2 XAS: Basic Principle

We recall here only the basic principles of the method. For a general review of X-ray absorption, the reader is referred to specialised books such as that of Köningsberger.[1] The interaction of X-rays with matter underlying XAS is described in a recent lecture of Cartier dit Moulin.[2] The basic process is the excitation of electrons from deep core levels of a selected atom by the absorption of

a photon (photoelectric effect). When the photon energy $h\nu$ is larger than the binding energy of the deep core level E_{binding}, an electron of this level can be promoted to an empty state. If $h\nu$ is larger than $E_{\text{binding}} + \Phi$, where Φ is the work function of the solid (energy required to promote an electron of the solid from the Fermi level to the vacuum level), a photoelectron can be emitted in the continuum, with a kinetic energy $E_{\text{kinetic}} = h\nu - (E_{\text{binding}} + \Phi)$.

In the frame of the electric dipolar approximation, the selection rules ($\Delta l = \pm 1$) dictate that an excited $1s$ core electron is sent to an empty state with p symmetry, and that a $2p$ core electron is excited into empty s or d states.

Figure 1 shows, as an example, the Si K absorption edge in SiO_2, which corresponds to excitation of a Si $1s$ electron into empty p states.[3] The absorption coefficient measured as a function of photon energy increases sharply when $h\nu$ becomes equal to the binding energy of the Si K level. This is the absorption edge. Usually two domains are considered, depending on the photoelectron kinetic energy. If the photoelectron is excited into the continuum with a high kinetic energy (e.g. larger than 50 eV), then the inelastic mean free path of the photoelectron is small.[4] The corresponding region of the absorption spectrum (starting from about 50 eV above the edge) shows oscillations, the intensity of which decreases with photon energy. These are called Extended X-ray Absorption Fine Structure (EXAFS) oscillations. EXAFS is sensitive to the short range order and gives the radial interatomic distance distribution function around the absorber up to 4 or 5 Å. At low kinetic energy (less than 50 eV), the mean free path of the photoelectron is large, and the photoelectron can be scattered by atoms located at larger distances and/or scattered many times (multiple scattering regime). This part of the spectrum is called XANES (X-ray Absorption Near Edge Structure). Very often, the study of these two parts of the spectrum is complementary, and one uses only the acronym XAS.

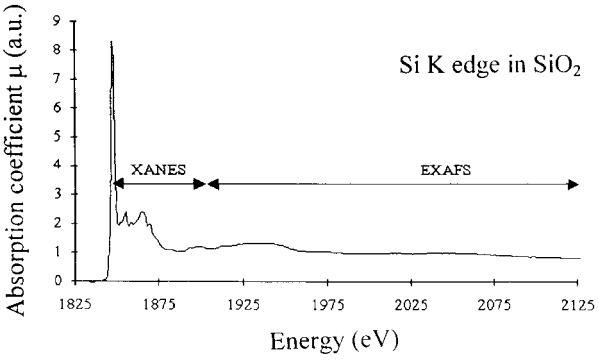

Fig. 1. Si K edge in α-quartz.[3]

3 XAS: Data Collection

An XAS experiment consists in measuring the X-ray absorption function versus photon energy in the vicinity of an atomic threshold. A synchrotron light source is needed because of the tuneable energy and high intensity required.

X-rays can be monochromatised with crystal monochromators or with gratings.[5,6] Data collection can be performed in two modes: either scanning energy mode or energy dispersive mode.

In the first case, energy scanning is obtained from a mechanical step-by-step rotation of the monochromator. The most simple experiment is a transmission experiment across a thin foil (thickness t), in which one measures the I/I_o ratio, where I is the intensity transmitted by the sample, and I_o the intensity of the incident beam. According to the attenuation law $I = I_o \exp(-\mu t)$, $\ln(I/I_o)$ is proportional to the absorption function μ. The transmission mode, standard for hard X-rays, is limited to very thin foils. Usually, the thickness x of the sample has to be adjusted such as $\mu.x = 1$, where μ is the absorption cross-section at the energy of interest. The absorption cross-sections of elements can be found in the tables of Ref. 7. For soft X-rays, in order to obtain a detectable signal, the sample has to be as thin as typically 0·1 μm, which sets technological problems for most materials. As an alternative, other detection modes can be used like the detection of the electrons or of the fluorescence photons, emitted as a result of the decay of the core hole. Under proper conditions, the total electron yield and the fluorescence yield can be considered to vary like the absorption coefficient.[8] The fluorescence yield technique is well suited to the study of thin and dilute samples. Owing to the small mean free path of electrons, the electron yield detection is more sensitive to the surface layers. In the case of insulating samples, charging effects under the photon beam may make it difficult to use electron detection, so that the fluorescence detection mode is preferred. In the scanning energy mode, the time necessary to register a spectrum is always limited by the time taken to rotate the monochromator at each step.

To reduce the recording time, which is essential for real time studies of dynamic phenomena such as phase transformations, an alternative mode is used: the energy dispersive mode.[9] An energy dispersive spectrometer is a transmission spectrometer allowing rapid XAS spectrum recording. The white radiation is dispersed by a focusing dispersive optics (a bent single crystal), which focuses the beam on the sample. The transmitted XAS signal is collected by a photodiode array, which is a position sensitive detector, in which each of the

sensing elements (e.g. 1024) measures the transmitted intensity at a photon energy fixed by its position. Then the whole XAS spectrum is recorded simultaneously, without any mechanical movement, so that the energy scale is very stable, which allows accurate and reliable detection of small changes in a series of closely related samples, as is the case in magnetic studies using circularly polarised X-rays[2] and structural determination under high pressure.[10] Compared to the scanning energy mode, the recording time is decreased. Another advantage of the energy dispersive mode is that, thanks to the focalisation, very small samples ($<0{\cdot}5\,\mathrm{mm}^2$) can be studied. One of the most important limitations however, is that only the transmission detection mode can be used in dispersive XAS.

Synchrotron radiation offers the possibility of producing either linearly polarised or circularly polarised X-rays, which can be used for X-ray magnetic circular (or linear) dichroism experiments (X-MCD or X-MLD). In X-MCD, one measures the difference in the absorption cross-section for right- and left-circular polarisation. This technique is valuable to study ferromagnetic materials, as one probes the local magnetic moment $\langle \mathrm{M} \rangle$. X-MLD is the difference in absorption cross-section for light polarised perpendicular or parallel to the magnetic moment and depends on $\langle \mathrm{M}^2 \rangle$ of the ions, and can be used in any system with collinear magnetic ordering, even antiferromagnetic.[6]

4 EXAFS: Application to Ceramics

From the absorption coefficient $\mu(E)$ the EXAFS function $\chi(k)$ is obtained from the expression $\chi(k) = (\mu - \mu_o)/\mu_o$, where μ and μ_o are the X-ray absorption coefficients for the sample and the isolated atom, respectively. Schematically, there exist two approaches to interpret the EXAFS data. In any case, the essential point for extracting the maximum of information from the EXAFS data is to get the best signal/noise ratio.

4.1 The standard EXAFS data processing

The basic interpretation of the EXAFS signal relies on single scattering of the wave associated to the emitted photoelectron by the neighbouring atoms. A classical procedure consists in deriving, from the EXAFS function, partial EXAFS spectra corresponding to the successive shells j of neighbours around the absorbing atom.[11] These partial EXAFS spectra are then simulated so as to obtain the structural parameters of each shell: R_j (average coordination distance from the absorbing atom to the neighbouring atoms in the jth coordination shell), N_j (the number of atoms in the jth shell at the average distance R_j) and σ_j (σ_j^2 represents the variance at distance R_j and contains the contribution from both static disorder and thermally induced vibrational displacements within a shell of neighbours). More precisely, the EXAFS function is written as the sum of contributions of the different coordination shells j:

$$\chi(k) = -\Sigma\left(N_j/kR_j^2\right)|f_j(k, R_j)|\, \mathrm{e}^{-2k^2\sigma_j^2}\mathrm{e}^{-2R_{j/}\lambda} \sin\left(2kR_j + \Phi_j(k)\right) \quad (1)$$

where $k = \sqrt{\frac{2m(E-E_o)}{\hbar^2}}$ is the electron wave vector and E_o the edge energy.[12] Here m and $\hbar$ are the electron mass and Planck's constant divided by 2π, $\Phi_j(k)$ represents the phase shift, $f_j(k, R_j)$ is the backscattered amplitude and λ the mean free path of a photoelectron. The chemical transferability principle states that phase shifts and backscattered amplitudes mainly depend on the central and neighbouring atoms, and are independent on the environment in the condensed state, so that they can be determined either by calculation or from reference samples. From $\chi(k)$ it is possible to derive a pseudoradial distribution function around the excited atom, $F(R)$, which is the modulus of the complex Fourier transform of $\chi(k)$. This function displays a series of peaks, whose positions are related to the coordination distances R_j, shifted by the phase shift $\Phi_j(k)$. Selecting a shell on $F(R)$, the back-Fourier transform to k space yields a partial EXAFS spectra, which can be fitted using the phase and amplitude functions derived from the EXAFS data of the reference material, leading to R_j, σ_j and N_j. It is important to note that σ_j and N_j are correlated parameters.

At this step, it is worth mentioning that the experimental EXAFS signal probes a mean local order. Indeed, if different types of sites exist in the material, then the structural parameters deduced from the EXAFS analysis will be an average of the parameters of the individual sites. This is why such a method is restricted to the study of single-phase materials. Moreover, in the case of strongly disordered materials (large σ values), the above procedure relying on expression (1) is no more valid, and one has to use a cumulant expansion of the EXAFS function.[11] In the case of EXAFS at the cation edges of ceramic oxides, the EXAFS signal is very weak, because of the low coordination number N_j of the absorbing atom, and the low backscattering factor of the oxygen atoms. Moreover, the transferability of phase and amplitude factors in the case of oxygen atoms is only an approximation.[13–15]

The standard EXAFS data processing has been successfully used to study the defect structure in ceramics, especially in the case of doping. For instance, the local structural environment around Y^{3+} and Zr^{4+} in Y_2O_3-ZrO_2 solid solutions was investigated,[16–18] as well as the effect of other dopants on zirconia stabilisation,[19] or the modification of local order in Y_2O_3 produced by oxygen vacancies.[20] We report below an EXAFS study of the local order in Ce doped Y_2O_3 ceramics.[21]

Ce doped Y_2O_3 ceramics (5 and 13 atm %, respectively labelled YCe5 and YCe13) were studied by EXAFS at the Ce L_3 edge (5724 eV), in the total electron yield detection mode, with the aim of determining the local order around the Ce atoms. For all experimental details (sample preparation, data collection…) the reader is referred to the original paper.[21] The X-ray diffraction spectra recorded prior to the EXAFS study exhibited the lines characteristic of solid solutions with C-type structure (Y_2O_3 structure). In Y_2O_3, all Y atoms are surrounded by a first shell of 6 oxygen atoms, at a mean distance of 2·28 Å. These oxygen atoms are located at the vertices of a cube, from which two are vacant. More exactly, there are two types of Y sites Y_I and Y_{II} depending on the location of the vacant oxygen sites, but the experimental EXAFS signal yields an average of the two individual sites. In the CeO_2 cubic structure (fluorite), the Ce atoms are surrounded by a first shell of 8 oxygen atoms at 2·34 Å, with a perfect cubic symmetry. Figure 2 shows the amplitude of the Fourier transform of the EXAFS function of the Ce L_3 edge in Ce doped Y_2O_3, together with that of a reference spectrum of CeO_2. The first large peak at ~2Å in the figure is related to the first oxygen coordination shell around Ce, while the second one (3–4 Å) is related to the second coordination shell, made of cations. Standard data analysis of the first coordination shells showed that there were 8 oxygen atoms around the Ce atoms (instead of 6 around Y in the Y_2O_3 structure), at a mean distance of 2·27 Å (the same as the Y–O distance in Y_2O_3). Analysis of the second coordination shell in the doped samples showed that there were 12 cation neighbours, at a distance 3·75 Å from the probed Ce atom, the same distance as the first Y–Y distance in the Y_2O_3 structure. Then these EXAFS results showed that the Ce atoms were substituted for Y in the Y_2O_3 structure, the additional O atoms around Ce occupying the intrinsic vacancies of the Y_2O_3 structure. This example shows how useful EXAFS can be for determining the defect structures in ceramics, especially in the case of doping or impurities.

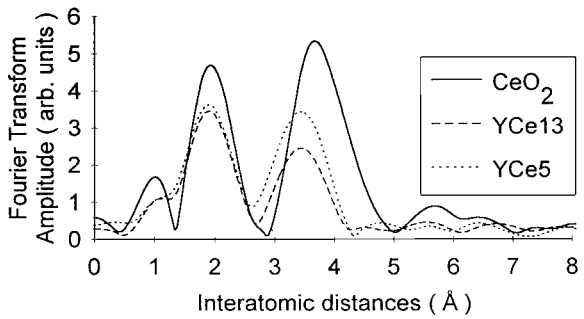

Fig. 2. Amplitude of the Fourier transform of the EXAFS function of the Ce L_3 edge in Ce doped Y_2O_3 (YCe5: 5 atm%; YCel3: 13 atm%), compared to that of CeO_2.[21]

4.2 The *ab initio* approach

An alternative approach to the standard data processing consists in performing an *ab initio* calculation of the EXAFS spectrum by assuming a given local structure around the absorbing atom, and comparing the theoretical spectrum with experiment. This can be done, e.g., by multiple scattering calculations.[22] This approach has the advantage of making it possible to take into account the contribution of multiple scattering contributions in the EXAFS spectrum, which are neglected in the standard analysis of EXAFS data we describe above. It has been shown in some cases that taking into account multiple scattering contributions allows the extension of the analysis of the EXAFS data well beyond the second shell.[23] This approach has proved to be very useful in a dynamic study of the phase transition mechanism $\alpha \rightarrow \beta$ of PbO.[24]

The aim of this study was to evaluate how XAS could bring new structural data complementary to those classically obtained by diffraction methods to study phase transitions.[24] Lead monoxide PbO was chosen because the tetragonal form α undergoes important local structure modifications during the phase transition to the orthorhombic form β. Moreover, the phase transition occurs at ambiant pressure at 490°C, which is an easily achievable temperature in an experiment.

Both PbO forms are layered structures consisting of PbO_4 pyramids arranged in planes perpendicular to the (001) direction. In the α form, the pyramids are symmetric with four identical Pb–O distances at 2·30 Å. In the β form, they are distorted, with two Pb–O distances at 2·21 Å and two at 2·48 Å (Fig. 3).

The phase transition was followed by recording EXAFS spectra (dispersive mode) at the Pb L_{23} edge (13050 eV). A constant heating kinetics of $10°C\,min^{-1}$ was kept. A full EXAFS spectrum was collected every minute, that is every 10°C. The acquisition time was equal to 4·8 s. Such a time resolution was imposed by the minimal signal to noise ratio allowing the processing of EXAFS data. The profile of the EXAFS curves in the range 138–517°C, surrounding the expected $\alpha \rightarrow \beta$ phase transition is displayed in Fig. 4. A detailed exam-

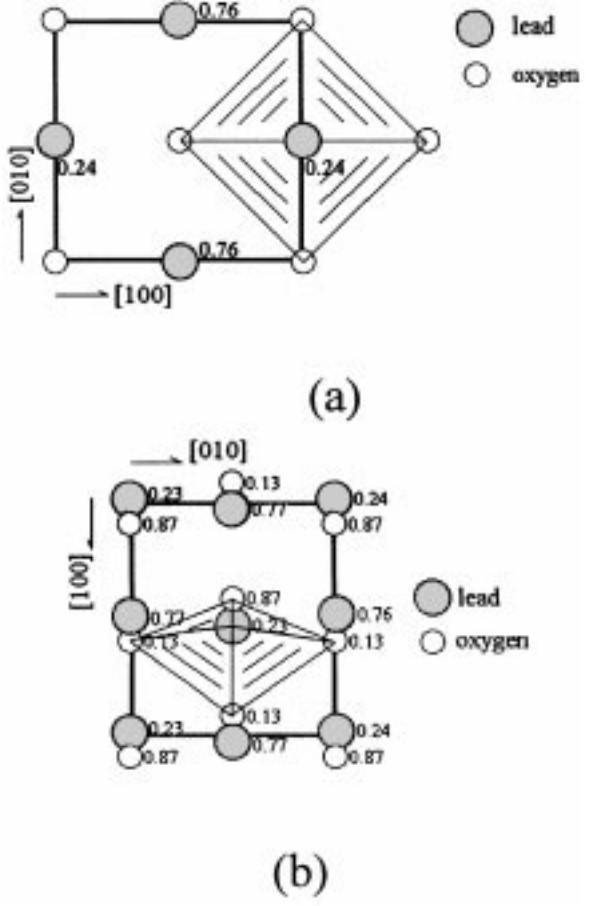

Fig. 3. (a) Projection of the PbOα structure along the [001] direction. (b) Projection of the PbOβ structure along the [001] direction. Numbers represent the z-coordinate.[24]

ination of the EXAFS spectra shows that the oscillation at $k \sim 4$ Å^{-1} is not altered when crossing the transition temperature but a continuous modification at k around 6·5–7·5 Å^{-1} is observed. The concavity of the curve is indeed progressively reversed.

To interpret these data, simulation of the EXAFS spectra of PbO α and β was done using the FEFF code.[22] Single and multiple scattering calculations were performed on clusters of increasing size centred around Pb (Fig. 5). It was checked that the calculations correctly described the experimental reference spectra recorded at the beginning of the heating process (α phase, 100 °C) and at the end (β phase, 692 °C). In both cases, the EXAFS oscillations mainly depend on single scattering diffusion on the first oxygen coordination shell that is inside the pyramidal structural unit PbO_4.

The second coordination shell made of Pb atoms significantly contributes to the amplitude of the first EXAFS oscillation at about 4 Å^{-1} and also to the shape of the EXAFS curve for high k values. The amplitude of this first oscillation is noticeably smaller for PbO β than for PbO α.

For PbO α, only the first oxygen coordination shell significantly contributes to the EXAFS signal in the k-range 6·25–7·25 Å. The strong EXAFS amplitude weakening observed in this k-range for PbO β is due to beat patterns produced by the superposition of the two different (Pb–O) scattering shells characteristic of the β crystallographic structure.

Using linear combinations of the α and β calculated spectra of Fig. 5, it could be verified that the experimental spectra obtained above the transition temperature were not characteristic of a mixture of the α and β phases, but really of a progressive phase transformation. The fact that the first

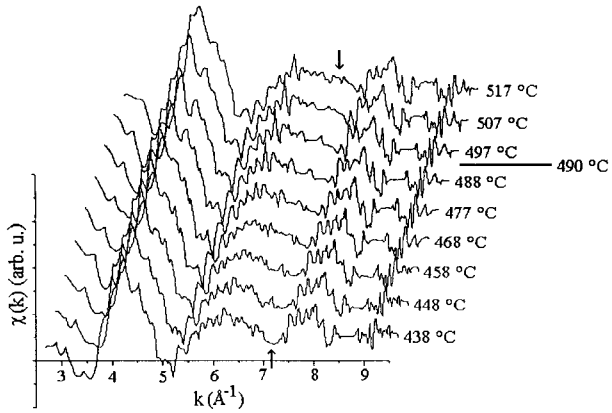

Fig. 4. Pb L_3 EXAFS curve profile of PbO in the temperature range 438–517°C obtained after a time smoothing procedure. The expected phase transition temperature of 490°C is shown.[24]

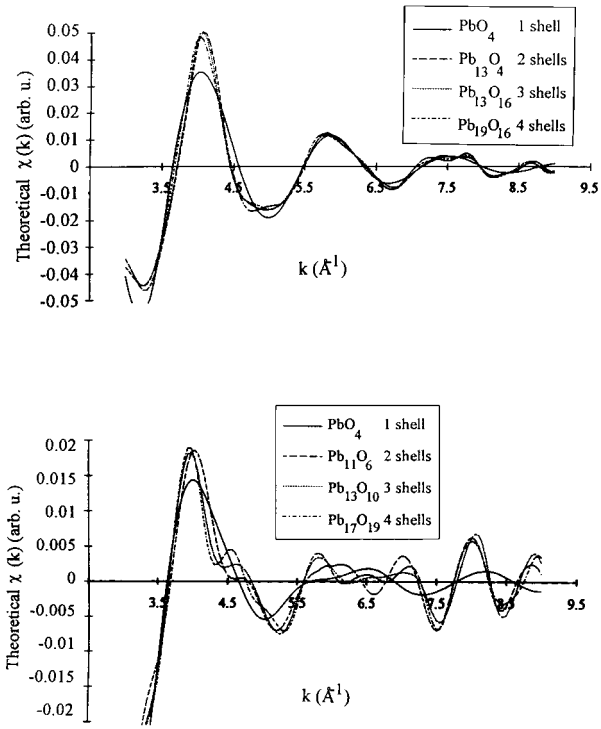

Fig. 5. Theoretical XAS curves obtained by FEFF5 code for PbOα, for cluster sizes varying from PbO_4 to $Pb_{19}O_{16}$ (upper panel) and for PbOβ, for cluster sizes varying from PbO_4 to $Pb_{17}O_{19}$ (lower panel).[24]

oscillation at ~4 $Å^{-1}$ is not changed means that, in a first step, the Pb atoms do not move. On the other hand, the decrease of the oscillation at ~7 $Å^{-1}$ means that the pyramids made of oxygen atoms are distorted first.

This time resolved XAS study of the polymorphic transformation of tetragonal to orthorhombic PbO gives evidence for a dynamical two-step transformation. The phase transition seems to be initiated by O atom displacements within the PbO4 pyramidal unit. The displacement of Pb atoms, caused by anion displacement, should occur in a second stage of the transformation. This study illustrates the possibilities of time resolved XAS spectroscopy to study solid state mechanisms such as phase transitions in ceramics. Great improvement in time resolution and signal to noise ratio can be expected from both the recent high flux storage rings and the constant improvements of detection systems.

5 XANES: Application to Ceramics

While EXAFS is mostly used for structural purposes, XANES brings information on both the local order and the electronic structure, which are strongly interconnected, so that electronic structure calculations are necessary to interpret the spectra. A very complete review on XANES of transition metals and their compounds, including ceramics in which the cation is a transition metal, has been written by F. M. F. De Groot,[6] who presented also the different electronic structure models relevant to describe the absorption spectra at the different edges. A more recent review of XANES investigations of transition metal oxides, nitrides, carbides can be found in Ref 25. In the present paper, we will focus on iron oxides α-Fe_2O_3, Fe_3O_4 and FeO.

α-Fe_2O_3 (corundum structure with formally Fe^{3+} ions) and FeO (NaCl structure with Fe^{2+} ions) are antiferromagnetic insulators in which the iron sites are nearly perfect octahedra. Fe_3O_4 is a ferrimagnetic semiconductor with distorted octahedra and tetrahedra with formally Fe^{2+} and Fe^{3+}. This family of compounds is then well suited to evaluate the influence of both the local structure around the iron atoms and the valence on the absorption spectra.

Whatever the excited atomic level, the near edge part of the XAS spectrum corresponds to a kinetic energy of the photoelectron smaller than 50 eV, hence to a large value of the inelastic mean free path. Therefore multiple scattering events occur between the wave associated to the photoelectron and those scattered by the neighbouring atoms.

5.1 The K absorption edges

The one electron approximation, in which one considers that all the electrons of the system remain passive during the absorption process, is usually valid for describing the K XANES spectra, in which one electron of the 1*s* level is promoted to a final state with *p* symmetry. These can be modelled either by band structure calculations (periodic calculation based on the unit cell of the crystal), or multiple scattering calculations (performed on a cluster centred on the excited atom). The core hole has to be introduced in the calculations, that is one should calculate the distribution of empty states in the final state of the absorption process. Comparing the ground state density of states directly with the X-ray absorption spectrum is in general satisfying in the case of the oxygen K edge, because there is an effective screening of the 1*s* core hole state by the valence electrons, which are in the case of oxides predominantly O 2*p* electrons. However, the effect of the core hole can be to pull down states to the bottom of the bands.[6] In the case of the cation 1*s* edges, the core hole can have a very strong importance to describe the shape of the absorption spectra, as is the case for the Si K spectrum.[3]

One advantage of multiple scattering calculations is that they can be performed on clusters of growing size and it is very convenient to observe the theoretical changes when increasing the number of neighbours and scattering paths around the absorbing atom. Figure 6 shows the comparison between experimental and theoretical oxygen K edge absorption spectra (multiple scattering calculations performed on clusters centred around the central O atom).[26] The experimental spectra of the different oxides exhibit clear differences in the

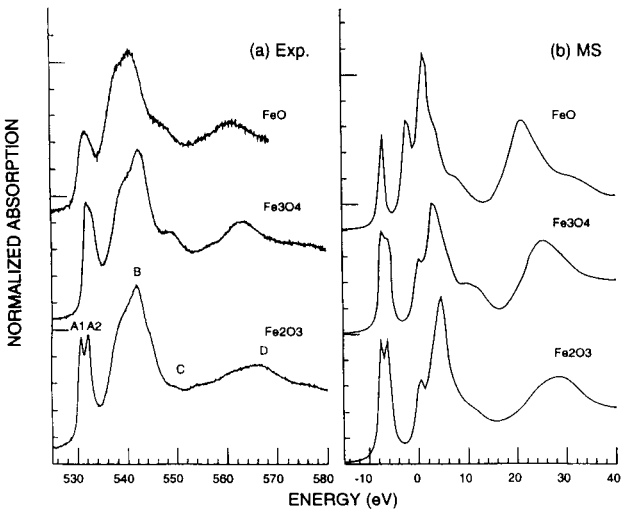

Fig. 6. Experimental (left panel) and theoretical (right panel) oxygen *K* edge absorption spectra of α-Fe_2O_3, Fe_3O_4, and FeO. The theoretical spectra were obtained by full-multiple scattering calculations performed on clusters centred around an oxygen atom.[26]

shape of the first peak A, as well as in the energy of peaks B, C and D measured from the edge. These changes are well accounted for by the calculations. By performing the multiple scattering calculations on clusters of increasing size, it is possible to discuss the origin of each structure of the spectrum with respect to the contribution of the different neighbouring shells of atoms. The near edge feature (doublet A_1-A_2 in α-Fe_2O_3, single peak A in Fe_3O_4 and FeO) is due to O 2*p*-Fe 3*d* hybridizations. The A_1-A_2 doublet of α-Fe_2O_3 is characteristic of the crystal field splitting for Fe^{3+} ions in octahedral site. The broad peaks B and D are due to diffusion by the first oxygen coordination shell while peak C originated from diffusion by the second oxygen coordination shell. For the other iron oxides, similar explanations can be drawn. A detailed discussion of these structures in terms of single and multiple scattering can be found in Ref. 26.

The Fe K edges of α-Fe_2O_3, Fe_3O_4 and FeO are shown in Fig. 7. In the iron oxide compounds with larger [O]/[Fe] ratio, the main peak broadens and shifts to higher energy. Moreover, a small prepeak at the low-energy side of the main peak clearly appears on the three spectra. Such prepeaks are observed in the K-edge of 3*d* transition metal oxides such as iron oxides and TiO_2. The origin of these structures is still debated.[6,28] In the case of the K edge of iron and for octahedral environment (FeO or α-Fe_2O_3), Chou et al interpreted the overall cross-section shape as originating from the coupling of the 4*p* partial wave of the central Fe with the 3*d* resonance of the neighbouring iron atoms.[29] The fine structure of the prepeak in some iron compounds has been shown to be characteristic of the tetragonal or octahedral coordination of iron.[30] Although there is not yet a consensus on the physical origin of the pre-peak, the preedge structures have been used to estimate quantitatively either the ratio of 4-fold iron to 6-fold,[30] or the $Fe^{3+}/\Sigma Fe$ ratio.[31] In this latter study, the

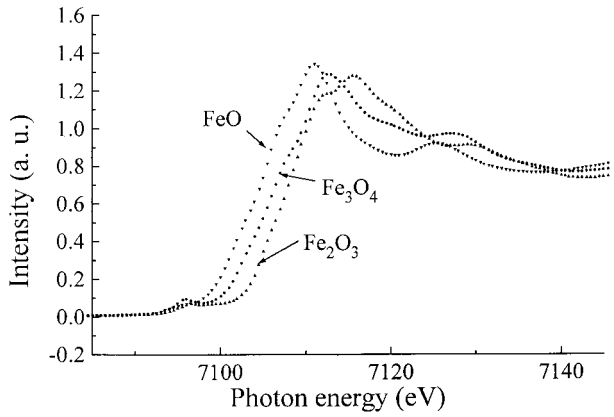

Fig. 7. Fe K absorption edges of α-Fe_2O_3, Fe_3O_4, and FeO.[27]

$Fe^{3+}/\Sigma Fe$ ratio was determined from the measurement of the energy shift of the pre-edge in reference compounds (Fig. 8).

5.2 The L_{23} absorption edges

When L_{23} (2*p*) edges are concerned, the monoelectronic approach is no more valid, because of electron-electron interactions. For instance, with a hole on the Fe 2*p* level, and a formal charge Fe^{3+}, we have to consider a transition of an initial state $/2p^6 3d^5>$ towards a final state $/2p^5 3d^6>$ (a hole on the 2*p* level, one more electron on the 3*d* level). There are several electronic configurations for each state, interacting with each other. To interpret the Fe L_{23} edges, it proved necessary to use configuration interaction methods which took into account the effect of the core hole, spin-orbit coupling, and multiplet effects.[6,32] In α-Fe_2O_3, all iron sites are 3+ octahedral. In FeO, they are all 2+ octahedral. The comparison between the experimental L_{23} edges with the theoretical ones obtained by the configuration interaction method (Fig. 9) clearly show the importance of the valence on the shape of the absorption spectra.[32] Indeed with close octahedral surroundings, the spectra of α-Fe_2O_3 and FeO are very different. These differences are due to the change in the number of occupations of the *d* orbitals (formally d^5 for Fe^{3+} and d^6 for Fe^{2+}), which leads to very different multiplets for d^5 to $2p^5 - d^6$ and d^6 to $2p^5 - d^7$ configurations. In Fe_3O_4, the situation is more complicated, as octahedral (Fe^{2+} and Fe^{3+}) and tetrahedral (Fe^{3+}) sites coexist, so that the experimental spectrum can only be reproduced by a summation of the different site theoretical contributions.[32] Fe L_{23} edges thus depends both on valence and structural environment.

Once the different absorption spectra at the O K and Fe L_{23} edges of α-Fe_2O_3, Fe_3O_4 and FeO are

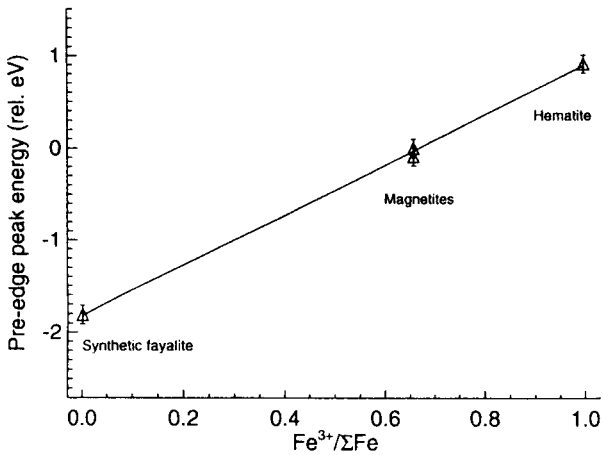

Fig. 8. Variation in the energy of the Fe K pre-edge, measured as a function of the $Fe^{3+}/\Sigma Fe$ ratio in reference compounds (after reference 31).

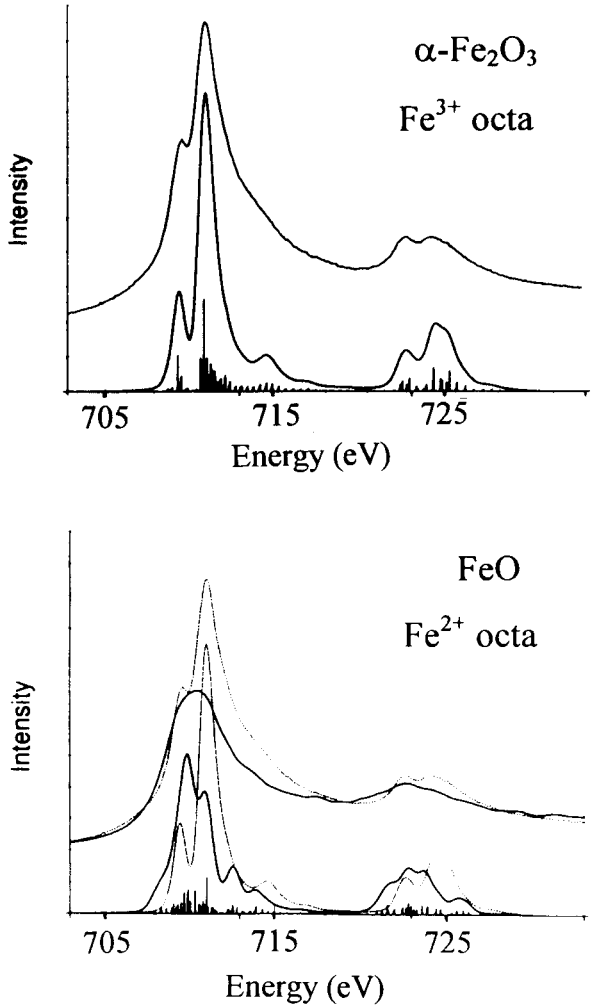

Fig. 9. Theoretical and experimental Fe2*p* X-ray absorption edge in α-Fe_2O_3 (upper panel) and FeO (lower panel). In each panel, the upper solid line indicates the experimental spectrum, the lower line is the calculation, the vertical bars are poles of the theoretical spectrum. In the lower panel, the dotted lines are those corresponding to α-Fe_2O_3, which are reported for comparison.[32]

interpreted, they can be used as a fingerprint of the different phases. In this way, the phase transitions in the surface layers of a α-Fe_2O_3 single crystal were followed as a function of different *in situ* (T, P_{02}) treatments leading to different stability domains of the iron oxide phase diagram.[33]

Magnetic dichroism, using the dependence of the absorption spectra on the polarisation of the X-rays, may give important additional information on the electronic structure. α-Fe_2O_3 (antiferromagnetic) exhibits, at $T_m \sim -10\,^{\circ}C$ (Morin temperature) a 'spin-flip' transition. Above T_m, the magnetic moments are perpendicular to the (0001) plane, while below T_m they lie in this plane. The spin orientation can thus be rotated with respect to the incident beam, by just changing the temperature while keeping the crystal in place. In this way, a magnetic linear dichroism was evidenced at the Fe L_{23} edge by Kuiper *et al.*,[34] using the total electron yield mode. More recently, the linear and circular magnetic dichroism of Fe_3O_4 (ferrimagnetic) was measured.[35] In this case, the sample was magnetized by an electromagnet. For all polarisation directions, the Fe L_{23} absorption edges were calculated, with atomic multiplet spectra for iron atoms. The best fits allowed the authors to derive a set of parameters, including e.g. the different crystal field splitting on octahedral and tetrahedral sites. This set of parameters was used to calculate MCD spectra of ferrites like $CoFe_2O_4$ and $Li_{0.5}Fe_{2.5}O_4$. Qualitative agreement with the experimental spectra suggests that the Fe 2*p* dichroism of other ferrites can be predicted.

5.3 New developments

Most of the examples above were obtained by using photon beams with a size of several mm^2 on the sample. One of the new developments of XAS concerns the microanalysis of materials. Micro-XANES would indeed give the ability to make measurements of the oxidation state of an element, as well as of its abundance in micrometer volumes. High brilliance sources and developments of X-ray optics make it possible to obtain focused X-ray microbeams (see, e.g. Ref. 36). As an example, the ratio $Fe^{3+}/\Sigma Fe$ could be determined in geochemical materials containing Fe with different oxidation states, at the Brookhaven Synchrotron Facility, with a $30 \times 50\,\mu m$ beam, from the study of the Fe K edges.[37] More recently, the charge-state ratios of iron in two phases in the mineral ilmenite $FeTiO_3$ could be quantified from micro-XANES experiments at the Fe L_{23} edges, compared to theoretical simulations of the spectra.[36] There is today great interest for such studies in the field of geochemical materials and environmental research, and there is no doubt that such a microanalysis tool could be profitable also in the field of ceramics.

6 Conclusion

Using a set of selected recent studies, we have shown what kind of information XAS is able to bring in the field of ceramics: structural information, but also information on the electronic structure around a given atom. One important asset of the method is its possible use in real-time studies, such as phase transformations induced by temperature. Besides the growing interest in dichroism experiments on magnetic materials, important developments of XAS in microanalysis of materials and especially ceramics are expected.

References

1. Köningsberger, D. C. and Prins, R., *X-ray absorption: Principles, Applications, Techniques of EXAFS, SEXAFS and XANES*, John Wiley and Sons, New York, 1988.
2. Cartier dit Moulin, C., Interaction of X-rays with matter: X-ray absorption spectroscopy. In *Magnetism and Synchrotron Radiation*, ed. E. Beaurepaire, B. Carrière and J. P. Kappler. Les Editions de Physique, Les Ulis, 1997, pp. 1–18.
3. Jollet, F. and Noguera, C., Core hole effect on the XAS Si K edge shape in α-quartz. *Phys. Stat. Sol. (b)*, 1993, **179**, 473–488.
4. Seah, M. P. and Dench, W. A., Quantitative electron spectroscopy of surfaces: a standard data base for electron inelastic mean free paths in solids. *Surf. Interf. Anal.*, 1979, **1**, 2–11.
5. Heald, S. M., EXAFS with synchrotron radiation. In *X-ray absorption: Principles, Applications, Techniques of EXAFS, SEXAFS and XANES*. John Wiley and Sons, New York, 1988, pp. 119–161.
6. De Groot, F. M. F., X-ray absorption and dichroism of transition metals and their compounds. *J. Electron Spectrosc. Relat. Phenom.*, 1994, **67**, 529–622.
7. McMaster, W. H., Kerr Del Grande, N., Mallet, J. H. and Hubbell, J. H., Compilation of X-ray cross-sections. UCRL-50174 Sec. II, Re. 1. Lawrence Radiation Laboratory, Univ. California, Livermore, California, 1969.
8. Stöhr, J., SEXAFS: everything you always wanted to know about SEXAFS but were afraid to ask. In *X-ray absorption: Principles, Applications, Techniques of FMAFS, SEXAFS and XANES*. John Wiley and Sons, New York, 1988, pp. 443–571.
9. Fontaine, A., Dartyge, E., Itié, J. P., Jucha, A., Polian, A., Tolentino, H. and Tourillon, G., Time-resolved X-ray absorption spectroscopy using an energy dispersive optics: strenghts and limitations. In *Topics in Current Chemistry*, Vol. 151. Springer Verlag, Berlin and Heidelberg, 1989, 179–203.
10. Itié, J. P., Polian, A., Martinez, D., Briois, V., Di Cicco, A., Filipponi, A. and San Miguel, A., X-ray absorption spectroscopy under extreme conditions. *J. Phys. IV France*, 1997, **7**, C2–31–C2-38.
11. Sayers, D. E. and Bunker, B. A., Data analysis. In *X-ray absorption: Principles, Applications, Techniques of EXAFS, SEX4FS and XANES*. John Wiley and Sons, New York, 1988, pp. 211–253.
12. Sayers, D. E., Stern, E. A. and Lytle, F. W., New technique for investigating non crystalline structures: Fourier analysis of the extended X-ray-absorption fine structure. *Phys. Rev. Lett.*, 1971, **64**, 1204–1207.
13. Eisenberger, P., Lengeler, B.Extended X-ray absorption fine structure determinations of coordination numbers: limitations. *Phys. Rev. B*, 1980, **22**, 3551–3562.
14. Pandya, K. I. and Köningsberger, D. C., Limitations in EXAFS amplitude transferability for low Z-scatterers. *Physica B*, 1989, **158**, 386–388.
15. Bunker, G., Transferability in XAFS. *Physica B*, 1989, **158**, 259–262.
16. Catlow, C. R. A., Chadwick, A. V., Greaves, G. N. and Moroney, L. M., EXAFS study of yttria-stabilized zirconia. *J. Am. Ceram. Soc.*, 1986, **69**, 272–277.
17. Li, P., Chen, I. W. and Penner-Hahn, X-ray absorption studies of zirconia polymorphs II effects of Y_2O_3 dopant on ZrO_2 structure. *Phys. Rev. B*, 1993, **48**, 10074–10081.
18. Thromat, N., Noguera, C., Gautier, M., Jollet, F. and Duraud, J. P., Electronic structure and atomic arrangement around Zr substituted for Y in Y_2O_3. *Phys. Rev. B*, 1991, **44**, 7904–7911.
19. Li, P., Chen, I. W. and Penner-Hahn, J. E., Effects of dopants on zirconia stabilization—an X-ray absorption study I trivalents dopants. *J. Am. Ceram. Soc*, 1994, **77**, 118–128; II tetravalent dopants. *J. Am. Ceram. Soc*, 1994, **77**, 1281–1288; III charge compensating dopants. *J. Am. Ceram. Soc*, 1994, **77**, 1289–1295.
20. Jollet, F., Noguera, C., Gautier, M., Thromat, N. and Duraud, J. P., Influence of oxygen vacancies on the electronic structure of yttrium oxide. *J. Am. Ceram. Soc.*, 1991, **74**, 358–364.
21. Douillard, L., Gautier, M., Thromat, N., Henriot, M., Guittet, M. J., Duraud, J. P. and Tourillon, G., Local electronic structure of Ce-doped Y_2O_3: an XPS and XAS study. *Phys. Rev. B*, 1994, **49**, 16171–16180.
22. Zabinsky, S. I., Rehr, J. J., Ankudinov, A., Albers, R. C. and Eller, M. J., Multiple-scattering calculations of X-ray absorption spectra. *Phys. Rev. B*, 1995, **52**, 2995–3009, and references therein.
23. Sikora, T., Hug, G., Jaouen, M. and Rehr, J. J., Multiple scattering EXAFS and EXELFS study of Al_3Ti and Ti_3Al alloys. *J. Phys. IV France*, 1997, **7**, C2 231.
24. Douillard, L., Gautier-Soyer, M., Duraud, J. P., Fontaine, A. and Baudelet, F., Time resolved study of a phase transition: the polymorphic transformation of tetragonal to orthorhombic PbO. *J. Phys. Chem. Solids*, 1996, **57**, 495–501.
25. Chen, J. G., NEXAFS investigations of transition metal oxides, nitrides, carbides, sulfides and other interstitial compounds. *Surface Science Reports*, 1997, **30**, 1–152.
26. Wu, Z. Y., Gota, S., Jollet, F., Pollak, M., Gautier-Soyer, M. and Natoli, C. R., Characterization of iron oxides by X-ray absorption at the oxygen *K* edge using a full multiple scattering approach. *Phys. Rev. B*, 1997, **55**, 2570–2577.
27. Gota, S., Jollet, F. and Gautier-Soyer, M., unpublished results.
28. Wu, Z. Y., Ouvrard, G., Gressier, P. and Natoli, C. R., Ti and O K edges for titanium oxides by multiple scattering calculations: comparison to XAS and EELS spectra. *Phys. Rev. B*, 1997, **55**, 10382–10392.
29. Chou, S. H., Guo, J. and Ellis, D. E., Electronic structure and X-ray absorption spectra of wüstite $Fe_{1-x}O$. *Phys. Rev. B*, 1986, **34**, 12–24.
30. Calas, G. and Petiau, J., Coordination of iron in oxide glasses through high-resolution *K* edge spectra: information from the pre-edge. *Solid State Commun.*, 1983, **48**, 625–629.
31. Bajt, S., Sutton, S. R. and Delaney, J. S., X-ray microprobe analysis of iron oxidation states in silicates and oxides using X-ray absorption near edge structure (XANES). *Geochimica et Cosmochimica Acta*, 1994, **58**, 5209–5214.
32. Crocombette, J. P., Pollak, M., Jollet, R., Thromat N. and Gautier-Soyer, M., X-rayabsorption spectroscopy at the Fe L_{23} threshold in iron oxides. *Phys. Rev. B*, 1995, **52**, 3143–3150.
33. Pollak, M., Gautier, M., Thromat, N., Gota, S., Mackrodt, W. C. and Saunders, V. R., An *in situ study of the surface phase transitions of* α-Fe_2O_3 by X-ray absorption spectroscopy at the oxygen *K* edge. Nucl. Instr. and Meth. in Phys. Res. B*, 1995, **97**, 383–386*.
34. Kuiper, P., Searle, B. G., Rudolf, P., Tjeng, L. H. and Chen, C. T., X-ray magnetic dichroism of antiferromagnet Fe_2O_3: the orientation of magnetic moments observed by Fe 2*p* X-ray absorption spectroscopy. *Phys. Rev. Lett.*, 1993, **70**, 1549–1552.
35. Kuiper, P., Searle, B. G., Duda, L. C., Wolf, R. M. and Van der Zaag, P. J., Fe L_{23} linear and circular magnetic dichroism of Fe_3O_4. *J. Electron Spectrosc. Relat. Phenom.*, 1997, **86**, 107–113.
36. Droubay, T., Mursky, G. and Tonner, B. P., High resolution X-ray absorption microspectroscopy of lamellar phases in natural ilmenite. *J. Electron Spectrosc. Relat. Phenom.*, 1997, **84**, 159–169.
37. Delaney, J. S., Bajt, S., Sutton, S. R. and Dyar, M. D., *In situ* microanalysis of $Fe^{3+}/\Sigma Fe$ in amphibole by X-ray absorption near edge structure (XANES) spectroscopy. In *Mineral Spectroscopy*: a tribute to Roger G. Burns, eg. M. D. Dyar, C. McCammon and M. W Schaefer. The Geochemical Society, Special Publication 5, 1996, pp. 165–171.